Pergamon

0277-5387(95)00256-1

Polyhedron Vol. 15, No. 4, pp. 705–715, 1996

0277-5387/96 $15.00 + 0.00

SYNTHESIS AND CHARACTERIZATION OF HOMO- AND HETEROPORPHYRIN DIMERS INVOLVING A RHODIUM–INDIUM BOND

A. G. COUTSOLELOS* and D. LUX

Department of Chemistry, Laboratory of Bioinorganic Coordination Chemistry, University of Crete, P.O. Box 1470, 71409-Heraklion, Crete, Greece

and

E. MIKROS

Pharmacy Department, Laboratory of Pharmaceutical Chemistry, University of Athens, Panepistimioupoli 15771-Zographou, Athens, Greece

(*Received* 13 *February* 1995; *accepted* 6 *June* 1995)

Abstract—The synthesis of a novel family of metalloporphyrin dimers containing a metal–metal (transition–non-transition metal) bond is presented. The reduction by $NaBH_4$ of the transition metal porphyrin complexes $(Por)Rh^{III}(Cl)$ generates the low oxidation state complexes $(Por)Rh^{I-}\ Na^+$, which by reaction with chloro-indium-porphyrin derivatives, $(Por)In^{III}(Cl)$, give rise to the above new family. By choosing the appropriate porphyrin ligand it is possible to vary the bond stability in these dimers systematically. The synthesis of porphyrin dimers involving rhodium–indium bonds, and their full characterization on the basis of ^1H NMR, UV–visible and FT-IR spectroscopy are described. A preliminary study of the photosensitivity of these complexes provides sufficient information about the stability of the metal–metal bond.

In recent years, there has been a remarkable development in the chemistry of metalloporphyrin† derivatives that show some degree of metal–metal interaction.[1] There is considerable interest not only in the synthesis of these compounds[2] but also in their biological significance,[3] and their potential use as starting materials for the synthesis of electron-conducting, stacked metal porphyrin polymers.[4]

The synthesis and characterization of different classes of metal–metal bonded metalloporphyrin dimers has been presented in the literature.[5] In general, when the nature of the porphyrin rings is different in the dimers, a polarity in the metal–metal bond is observed. A similar polarity has been detected for the unique bimetallic transition–non-transition porphyrin dimer, (OEP)Rh–In(OEP), which has been described in the literature.[6] The polarity of the bond is demonstrated by a regioselective addition of alkyl iodides.

In this paper, we report the syntheses, spectroscopic characterization and behaviour towards light irradiation, of a series of homo- and heteroporphyrine dimers containing the same metal–metal bond stabilized by the electron donor or electron acceptor ability of the corresponding macrocycle (TPP or OEP ring). This difference in stability can be attributed to various factors, such

* Author to whom correspondence should be addressed.

† Abbreviations used: $(Por)^{2-}$, $(TPP)^{2-}$, $(OEP)^{2-}$, $(TTP)^{2-}$, $(DPB)^{2-}$ dianions of a general porphyrin, 5,10,15,20-tetraphenylporphyrin; 2,3,7,8,12,13,17,18-octaethylporphyrin; 5,10,15,20-tetratolylporphyrin and 1,8-bis-[5-(2,8,13,17-tetraethyl-3,7,12,18-tetramethyl) porphyrin] biphenylene.

as its peripheral groups, the stereochemistry of the complex and the distance of the metal from the plane of the four nitrogen atoms.

EXPERIMENTAL

Chemicals

All chemicals were reagent grade and used without further purification except as noted below. Basic alumina type I was activated at 150 C. All solvents were distilled and dried with molecular sieves under a dry nitrogen or argon stream. All reaction procedures were carried out under argon. Ethanol was degassed by argon bubbling under ultrasound. The basic aqueous solution of $NaBH_4$ was degassed in the same way and was frozen three times at liquid nitrogen temperature under inert atmosphere in order to remove all traces of O_2.

Methods and instruments

All manipulations of oxygen- and water-sensitive materials was performed in a vacuum line under an atmosphere of purified Ar. UV–visible spectra were recorded on a Lambda-6 Perkin–Elmer spectrophotometer or on an ORIEL diode-array visible spectrophotometer, using 5×10^{-3} M solutions of toluene. Samples for IR measurements were prepared as 1% dispersions in CsI pellets or Nujol mulls and recorded on an FT-IR 1760 series Perkin–Elmer spectrophotometer. ^{1}H NMR spectra were recorded on a Bruker AC spectrometer (200 MHz for ^{1}H). Spectra were recorded for solutions in 2×10^{-3}M $CDCl_3$, with tetramethylsilane as internal reference.

Preparation and purification of the complexes

Rhodium(III) and indium(III) porphyrins. The introduction of indium and rhodium metal ions into the porphyrin rings was achieved following literature methods.[7,8]

Reduction of (Por)$Rh^{III}Cl$ *to* [(Por)Rh^{I}]$^-$. $NaBH_4$ (40 mg, 1.06 mmol) in 4 cm^3 of 0.5 N NaOH was added to a solution of 30 mg of (Por)Rh^{III}(Cl) (0.04 mmol) in 15 cm^3 of ethanol under argon.[2] The resulting mixture was stirred for 2 h at 60 C. The formation of rhodium(I) porphyrin was confirmed by UV–vis spectroscopy. The complex is reoxidized rapidly on exposure to air.

Preparation of (Por)Rh–In(Por) *or* (Por)Rh–In(Por)′. This preparation was modified with respect to the previously published procedure[6] as follows: (Por)In(Cl) was reacted directly with the [(Por)Rh^{I}]$^-$ anion, which was provided by the reduction of the (Por)RhCl by $NaBH_4$. The reaction solvent of the porphyrin solution of rhodium anion was evaporated *in vacuo* before the addition of 35 mg of (Por)In(Cl) in 15 cm^3 THF. The mixture was stirred for 0.5 h after which it was chromatographed on basic Al_2O_3, grade I, under an inert atmosphere, in the dark. The porphyrin dimer formed was eluted first with toluene [yield based on starting Rh porphyrin complex: (OEP)Rh–In(OEP) (**I**) 34%, (OEP)Rh–In(TPP) (**II**) 73%, (TPP)Rh–In(OEP) (**III**) 80%, (TPP)Rh–In(TPP) (**IV**) 38%, after recrystallization in benzene]. Found C, 67.2; H, 6.7; N, 8,7. Calc. for **I** $C_{72}H_{88}N_8RhIn$: C, 67.4; H, 6.9; N, 8.7%; Found C, 70.3; H, 5.3; N, 8,1. Calc. for **II** $C_{80}H_{72}N_8RhIn$: C, 70.5; H, 5.3; N, 8.2%; Found C, 70.4; H, 5.3; N, 8,2. Calc. for **III** $C_{80}H_{72}N_8RhIn$: C, 70.5; H, 5.3; N, 8.2%; Found C, 73.1; H, 3.8; N, 7,6. Calc. for **IV** $C_{88}H_{56}N_8RhIn$: C, 73.2; H, 3.9; N, 7.8%.

Photodecomposition. A solution of given concentration of homo- or hetero-porphyrin dimer was prepared and introduced in to a spectrophotometric cell. The samples were exposed directly to a Quartz Halogen Tungsten Lamp (ORIEL, 500 Watt). The light was delivered directly to the sample in the cell by fibre optic. Alternatively, a monochromator was used to resolve spectrally the light for irradiating at selected wavelengths in the region of the Soret band. The use of monochromatic irradiation caused a much slower dimer photodecomposition than white light. All manipulations were carried out in the dark. After irradiation, the samples were checked by UV-vis spectroscopy. The exposure time required for complete degradation differed between the investigated compounds.

RESULTS AND DISCUSSION

Synthesis

The syntheses of (Por)Rh–In(Por) and (Por)Rh–In(Por)′ are summarized in Scheme 1. The complexes formed are stable in the solid state but not in solutions exposed to light. In the range 4000–400 cm^{-1}, the IR spectrum is almost the "addition" of the spectra of the corresponding monomers. For all the complexes, no vibrations due to Rh—In bonds were observed, probably because of the low frequency of this type of vibrations, which must appear at values below 200 cm^{-1}. All UV–vis studies on dimeric porphyrins containing a metal–metal bond have been carried out in toluene. Table 1 summarizes the UV–vis data.

Dimers **III** and **IV**, which incorporate a (TPP)Rh unit, exhibit three maxima in the region of the Soret band and three others in the *Q* region (including

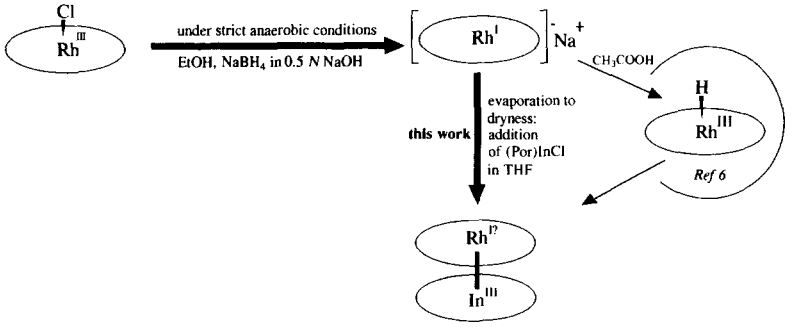

Scheme 1. Reaction processes in this paper compared with those in the literature.

Table 1. UV–vis data for complexes (Por)Rh–In(Por) and (Por)Rh–In(Por)′ (λ/nm, ε/dm^3 mol^{-1} cm^{-1} in parentheses) compared with data for their precursors

Compound	*B*-bands					*Q*-bands			Solvent
(OEP)Rh–In(OEP)	339sh	362	408			517	566sh	618	Toluene
(I)		(57.8)	(46.5)			(6.5)		(1.9)	
(OEP)Rh–In(TPP)	340	370	400sh	421	454sh	523		625	Toluene
(II)	(51.5)	(84.4)		(47.1)		(13.4)		(3.9)	
(TPP)Rh–In(OEP)	340	373sh	408			526	572	624sh	Toluene
(III)	(40.6)		(77.3)			(4.4)	(2.4)		
(TPP)Rh–In(TPP)	341	379		415		519	599	651	Toluene
(IV)	(36.8)	(64.8)		(115.2)		(6.9)	(3.2)	(2.1)	
(OEP)RhCl·2H$_2$O*	285	339	403			520	554		$CHCl_3$
from ref. 2	(4.17)	(4.26)	(5.12)			(4.12)	(4.40)		
(OEP)InCl		388	408			500	539	577	Benzene
from ref. 13a		(54)	(436)			(4)	(19)	(22)	
(TPP)RhCl				421			534	567	CH_2Cl_2
				(92.6)			(11.9)	(5.4)	
(TPP)InCl			404	426		515	559	600	Benzene
from ref. 13a			(47)	(570)		(6)	(21)	(10)	

* Values in log.

shoulders). Similar observations can be made for complexes **I** and **II**. This is characteristic of hyperporphyrins[9] compounds having a σ-bond between the metal and axial ligand.[10] Hyperporphyrins show prominent extra bands ($\varepsilon > 1000\ M^{-1}\ cm^{-1}$) in the region $\lambda > 320$ nm, where normal porphyrins show only *Q*, *B* and *N* (π, π^* bands). The maxima corresponding to the Soret region for the above complexes are almost identical in contrast to the *Q* region. The molar extinction coefficients for the new compounds are smaller than those for the initial complexes. The biggest molar extinction coefficient was measured for the (TPP)Rh–In(TPP) dimer.

Photodecomposition

Figure 1 shows the evolution of the photodegradation reactions for the four dimers (the region of the *Q*-bands has been multiplied by 10). Upon irradiation with white light, their metal–metal bond breaks to give five-coordinate complexes with chloro as axial ligands.[11] The UV–vis absorptions of these five-coordinate complexes are identical with the equivalent electronic spectra for the precursors of the dimers: (Por)Rh^{III}(Cl) and (Por)In^{III}(Cl). At the last step of each decomposition, indium(III) porphyrin: (Por)In^{III}(Cl) is the dominant detectable species, easily detected because of its larger molar extinction coefficient relative to the corresponding rhodium(III) derivative: (Por)Rh^{III}(Cl). However, in case (b) the Soret band of (OEP)Rh^{III}(Cl) appears next to (TPP)In^{III}(Cl) and in case (c) the Soret band of (TPP)Rh^{III}(Cl) is visible as shoulder of (OEP)In^{III}(Cl). In the other cases we detect rhodium(III) porphyrin by the second derivative of the observed spectrum. The UV–vis spectrum given by Wayland[6] and coworkers for (OEP)Rh–In(OEP), has maxima at 362,

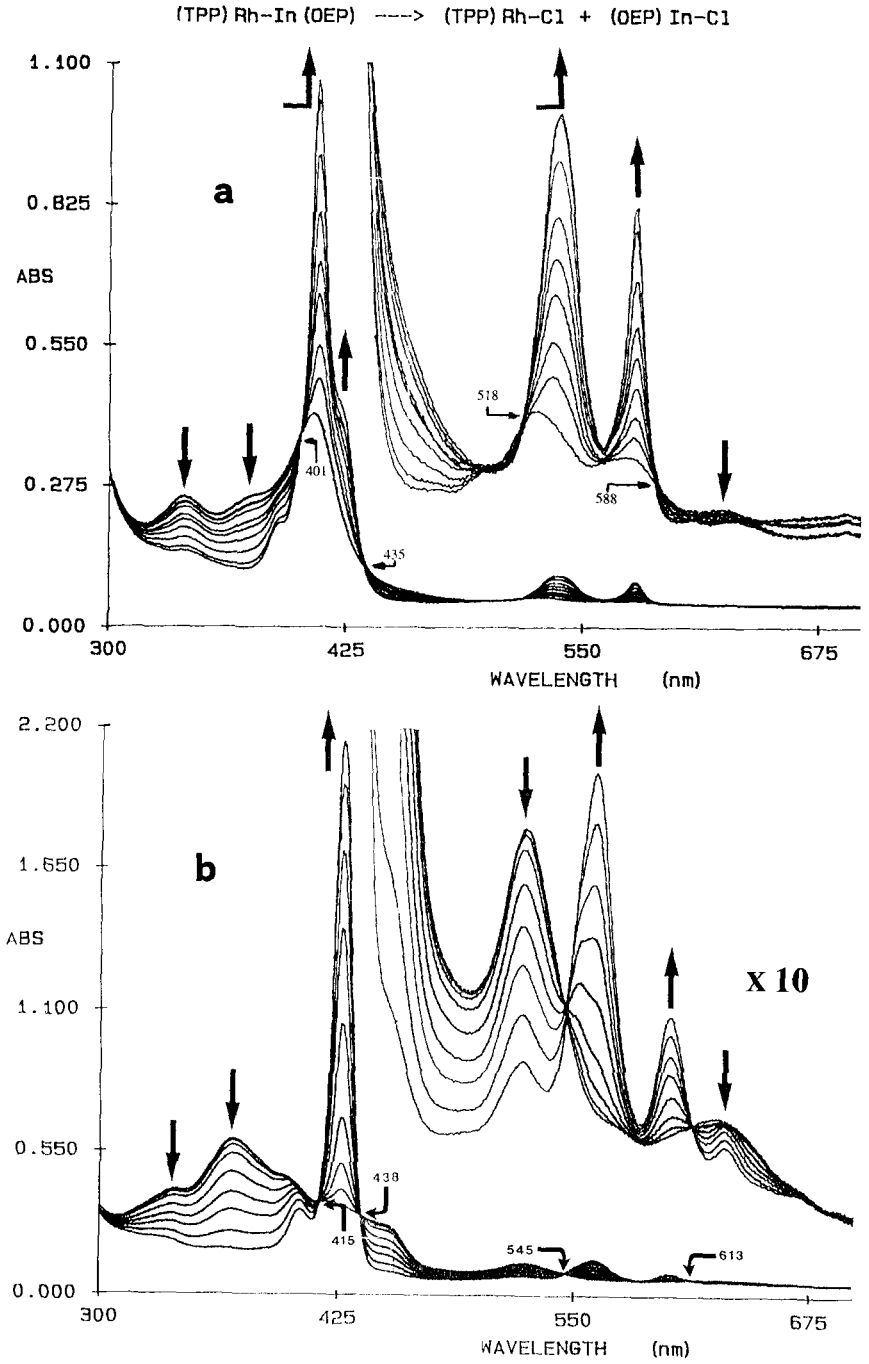

Fig. 1. UV–vis control for the photodecomposition of the four (Por)Rh–In(Por)′ and (Por)Rh–In(Por) dimers; a = (TPP)Rh–In(OEP, b = (OEP)Rh–In(TPP), c = (OEP)Rh–In(OEP) and d = (TPP)Rh–In(TPP).

392, 411, 522, 555sh, 579 nm in C_6H_6. In comparison with our corresponding values in toluene (Table 1) and its photodecomposition behaviour (Fig. 1) it is obvious that peaks the at 392 and 579 nm do not belong to the dimer but to (OEP)In(Cl), which is probably formed by minor decomposition of the starting material, (OEP)Rh–In(OEP).

A set of four isosbestic points is observed, as can be deduced from each spectrum (see Fig. 1). This means that for each photodecomposition there are no secondary reactions.

The photodecomposition rates give a good estimate of the metal–metal bond strength order if the reactions are under thermodynamic control, as we suggest. For an equivalent concentration of 10^{-6} mol l^{-1} in toluene, durations (in seconds) of

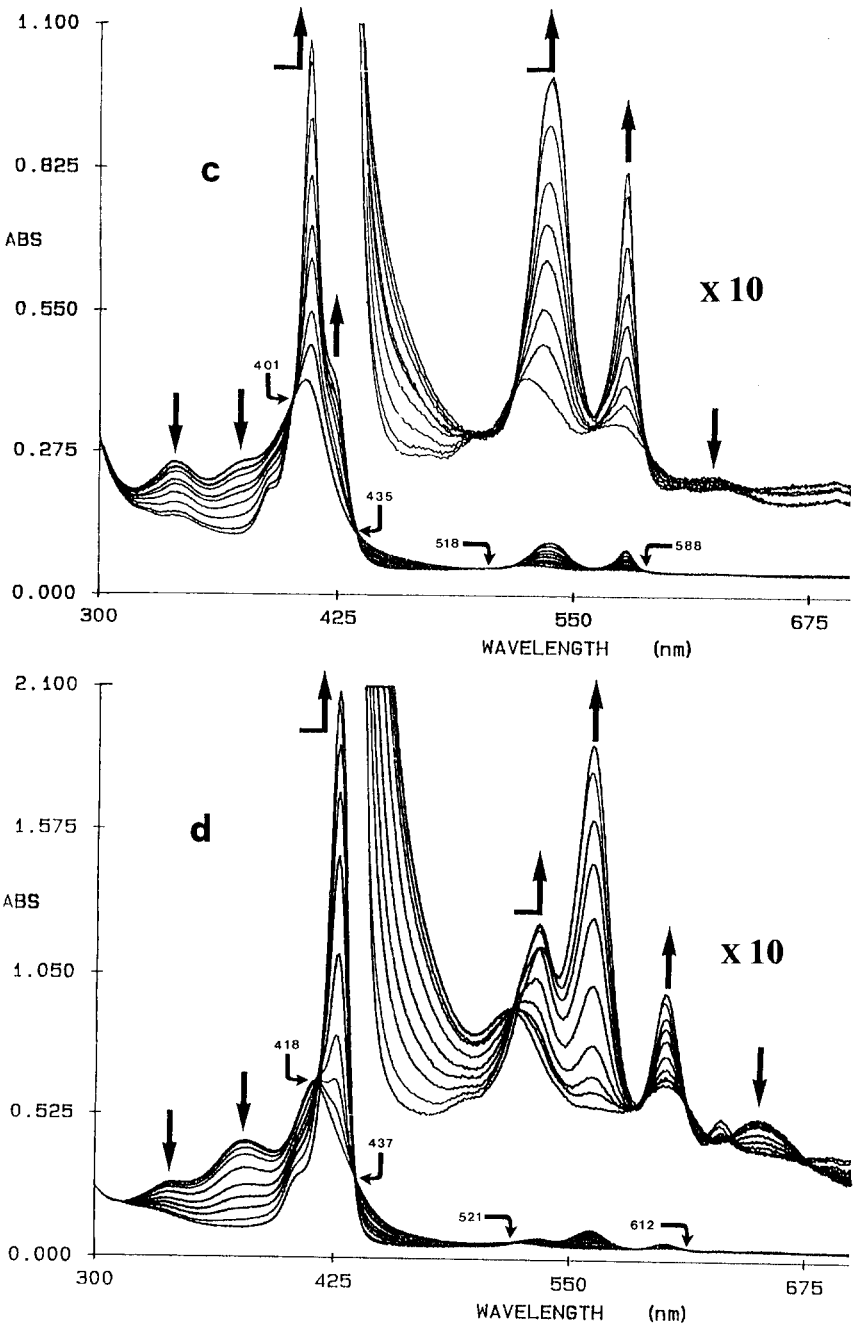

Fig. 1—*Continued.*

decomposition are as follows: (OEP)Rh–In(OEP) (**I**): 300 s < (TPP)Rh–In(OEP) (**III**): 700 s [2.3 × 300 s] < (OEP)Rh–In(TPP) (**II**): 940 s [3.1 × 300 s; 1.3 × 700 s] < (TPP)Rh–In(TPP) (**IV**): 1270 s [4.2 × 300 s; 1.8 × 700 s; 1.4 × 940 s].

The Rh—In bond is probably much more stable in the (TPP)Rh–In(TPP) dimer than in (OEP)Rh–In(OEP), because the excited state energy of OEP is higher than TPP. All other factors being constant, the decomposition times depend on the probability of the compound absorbing a photon (that is, it depends on its absorption coefficient) and on the relative stability of the metal–metal bond. (Here, we assume that the rate-determining step for the reaction is the bond-scission step, which is reasonable in view of the high reactivity of a produced intermediate radical). In order to assess the above factors, we have calculated the integrated absorption of the compounds, convoluted by the spectral output of the lamp. This parameter, increases in the

order **I** < **III** < **II** < **IV**, in the same order as the photostability of the compounds increases, with the exception of the relative stability of **II** and **III**. This strongly suggests that the observed photostability of the compounds relates to the thermodynamic stability of the corresponding M—M′ bond, and that if **I** has the weakest bond, **IV** has the strongest one. This assertion is not certain as far as the relative stability of compounds **II** and **III** is concerned; where decomposition rates are of the same order as their integrated absorptions (i.e. **II** faster than **III**). The metal–metal bond is strongest when TPP is attached to indium. This is understandable if the polarization $Rh(I)^- : \rightarrow In(III)^+$ is considered. The above data have also been confirmed by the action of various alkylhalogenides on these compounds.[11] Finally, we conclude that when the extinction coefficients decrease the Rh—In bond breaks down easily after irradiation.

In summary, for the four dimers the molar extinction coefficients increase as **I** < **III** < **II** < **IV**, as for their stability on exposure to light. This is extremely important because it establishes that the photodegradation rate does not follow the extinction coefficient. Therefore, the photodegradation order must represent metal–metal stability order. We note than no decomposition of the binuclear rhodium–indium porphyrin complexes by heating solutions in the dark has been observed.

^1H NMR

The proton NMR spectra were analysed considering that the presence of the two porphyrin rings creates two distinct regions *endo* and *exo* (Scheme 2). Table 2 summarizes the ^{1}H NMR data for the dimers **II**, **III** and **IV**, whereas the spectra of **III** and **IV** are illustrated in Fig. 2.

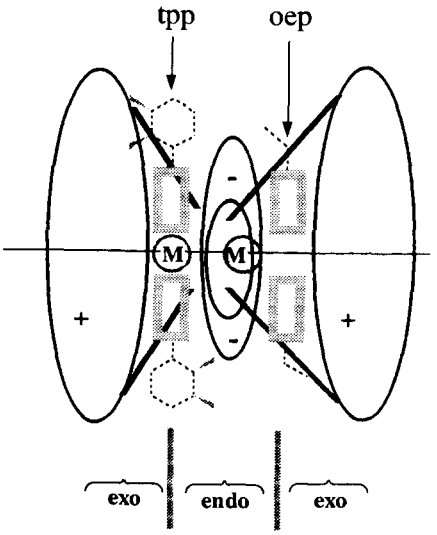

Scheme 2. The *exo*- and *endo*-regions.

The spectra of **II** and **III** consist of bands assigned to the phenyl group and the pyrrole protons of the TPP macrocycle and the *meso* protons and the β-ethyl substituents of the OEP macrocycle. The individual resonances could be assigned through the observation of well-resolved spin–spin splittings and 2D experiments. The two downfield singlets, attributed to the *meso*-OEP and pyrrole TPP, are differentiated by integration. The α-methylene proton resonances of the OEP ring are observed as two identical, coupled multiplets that indicate loss of the mirror symmetry in the plane of the porphyrins. This loss of symmetry, along with the slow rotation of the phenyl rings, causes the phenyl protons to be observed as a set of five well-resolved signals; one triplet of triplets exhibiting a 7 Hz *ortho* spin–spin splitting and a 1 Hz long-range *meta* coupling attributed to the *p*-phenyl proton, and two triplets of doublets, and two doublets of triplets exhibiting the same 7 Hz *ortho* coupling and 1 Hz *meta* coupling assigned to the *meta*- and the *ortho*-phenyl protons, respectively. The COSY LR confirms this assignment by showing correlations between 3- or 4-bond distance protons, e.g. the *p*-proton correlates with all four other phenyl protons and the *o*-proton shows connectivity with the *m*-, *o*′- and *p*-protons but not with the *m*-one (e.g. Fig. 3).

The distinction between the *ortho*, *ortho*′ and *meta*, *meta*′ pairs of protons requires consideration of the effects of the magnetic anisotropy of the porphyrin macrocycle and the metal–metal bond.[12,13] The *o*′- and *m*′-protons are *endo* oriented and experience a downfield deshielding relative to the monomer (Table 3), while the *o*- and *m*-protons are *exo* oriented and experience an upfield shielding. In particular, the *o*- and *o*′-protons are closer to the centres of the magnetic anisotropy and they experience more significant shifts than the *m*- and *m*′-protons.

For the phenyl protons, the magnetic anisotropy effects are more pronounced for the *o*- and *o*′-protons when they are attached to the In porphyrin, and less when they belong to the Rh one, but there is no significant difference for the *m*-, *m*′- and *p*-protons. The opposite is true for the pyrrole TPP and the *meso*-OEP protons. For the pyrrole TPP protons, an upfield shielding is more pronounced for the RhTPP porphyrin (complex **III**). The *meso*-OEP protons experience an upfield shielding as well, more important again for the Rh porphyrin. This leads to an unambiguous assignment of the spectra of **I**[6] and **IV** where the two porphyrin ligands for In and for Rh are identical. Proton chemicals shifts for compound **I** have been

Table 2. ^{1}H NMR data for complexes (Por)Rh–In(Por) and (Por)Rh–In(Por)′ in $CDCl_3$

Compound	Macrocycle								
	Tetraphenylporphyrin						Octaethylporphyrin		
	o-H (*exo*)	*o*′-H (*endo*)	*m*-H (*exo*)	*m*′-H (*endo*)	*p*-H	H-pyr	CH_2-	CH_3	H-*meso*
(I)*							m/16,	t/24,	s/4,
(OEP)Rh							4.25/3.89	1.78	8.78
							m/16,	t/24,	s/4,
(OEP)In							4.20/3.89	1.72	9.31
(II)							m/16,	t/24,	s/4,
(OEP)Rh							3.99/3.79	1.51	8.66
	d/4,	d/4,	t/4,	t/4,	t/4,	s/8,			
(TPP)In	6.95	9.24	7.37	8.19	7.76	8.37			
(III)	d/4,	d/4,	t/4,	t/4,	t/4,	s/8,			
(TPP)Rh	7.09	9.01	7.38	8.15	7.72	8.03			
							m/16,	t/24,	s/4,
(OEP)In							4.15/3.88	1.50	9.20
(IV)	d/4,	d/4,	t/4,	t/4,	t/4,	s/8,			
(TPP)Rh	7.19	8.78	7.42	7.85	7.69	8.14			
	d/4,	d/4,	t/4,	t/4,	t/4,	s/8,			
(TPP)In	7.07	9.01	7.42	7.89	7.73	8.44			
(TPP)InCl	d/4,	d/4,		m/4,		s/8,			
ref. 12	7.98	8.02		7.45		9.04			
(TPP)RhCl	m/4,			m/12,		s/8,			
ref. 12	8.25			7.77		8.94			
(OEP)InCl							m/16,	t/12,	s/4,
ref. 13a							4.03/3.90	1.83	10.39
in C_6D_6									
(OEP)RhCl							m/16,	t/12,	s/4,
ref. 2							4.13	1.98	10.32
in C_6D_6									

I* = (OEP)Rh–In(OEP), ref. 6; **II** = (OEP)Rh–In(TPP); **III** = (TPP)Rh–In(OEP); and **IV** = (TPP)Rh–In(TPP).

reported,[6] but were not attributed to any specific metalloporphyrin.

The NMR spectra of all the complexes consist of two sets of signals corresponding to the protons of the Rh and the In porphyrins. In the spectrum of **IV**, we observe two distinct singlets assigned to the pyrrole protons at δ8.44 and 8.14 and two series of *o*-, *o*′-, *m*-, *m*′- and *p*-doublets and triplets for the phenyl protons. The *o*- and *o*′-doublets are clearly observed but *m*-, *m*′-signals are overlapping, therefore the COSY LR spectrum (Fig. 3) is required for assignment of the different chemical shifts. The COSY LR permits us also to clarify the correlations between the resonance signals of the protons of the same phenyl ring and to distinguish between the two different phenyl rings. Our analysis proceeds as follows. First, the two doublets at δ9.01 and 8.78 are assigned to the *o*′-protons of the In and Rh macrocycles with respect to the spectra of **II** and **III**. The 2D spectrum indicates that the *o*′-proton at δ9.01 correlates with the *m*′-proton at δ7.89, the *o*-proton at δ7.07 and the *p*-proton at δ7.73. From the connectivities of the *p*-proton we assign the *m*-protons at δ7.42. The *o*′-proton at δ8.78 also shows cross-peaks with the *m*′-proton at δ7.85, the *o*-proton at δ7.19 and the *p*-proton at δ7.69, while the *m*-protons at δ7.42 are also assigned from their connectivities. According to the discussion concerning the complexes **II** and **III**, the first set of phenyl signals, with higher shielding of the *o*-proton and deshielding of the *o*′-proton, are assigned to the In macrocycle. The comparison between **II** and

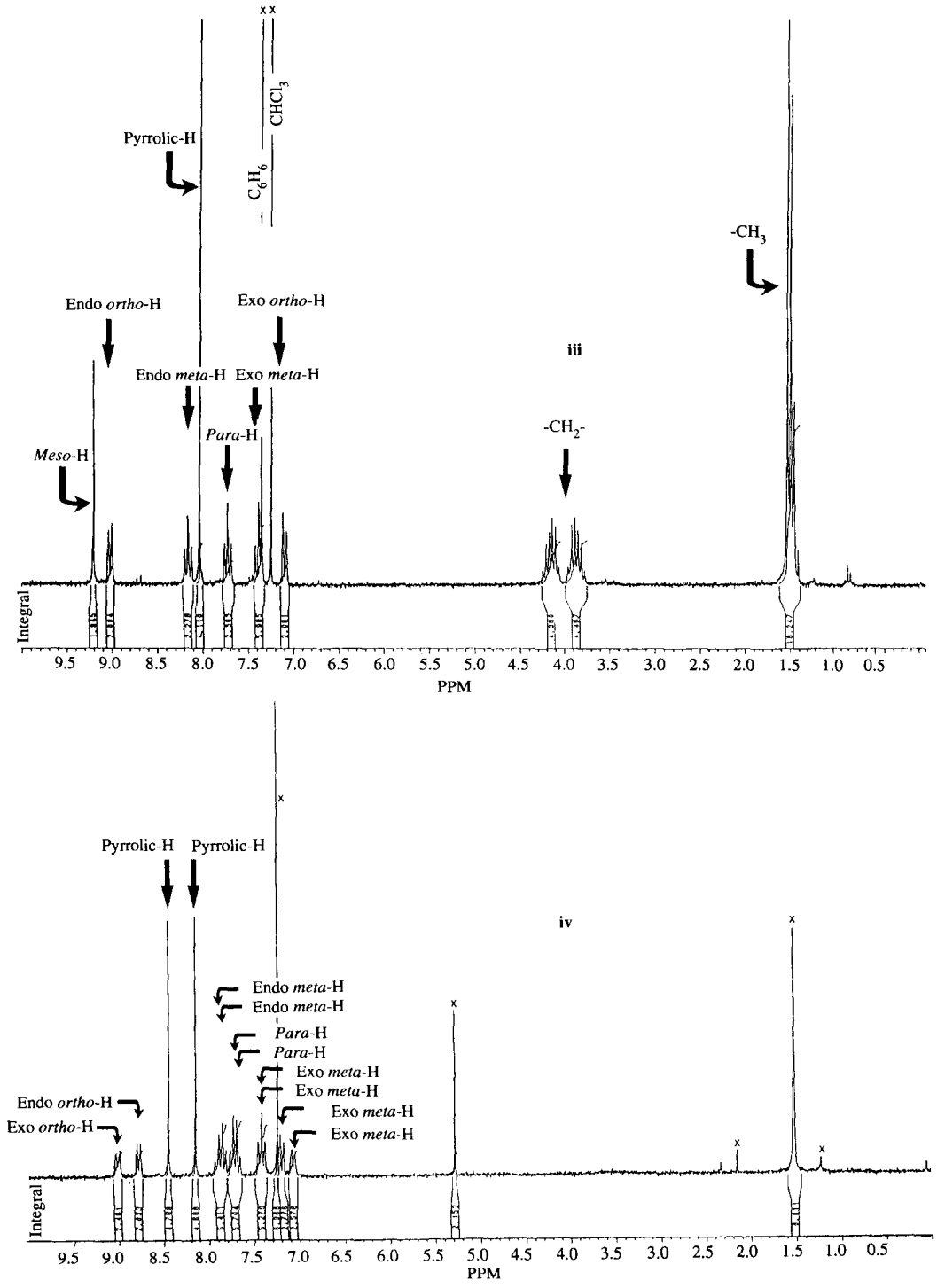

Fig. 2. ^{1}H NMR spectra of complexes **III** and **IV** in $CDCl_3$.

III leads us also to assign the singlet at δ8.44 to the pyrrole protons of the same porphyrin macrocycle. The seconds set of signals are then assigned to the protons of the Rh porphyrin.

By the same procedure, the (OEP)Rh and (OEP)In signals of the spectrum of complex **I** are distinguished based on comparison of **I** with **II** and **III**. Thus, the singlet at δ9.31 is assigned to *meso*-protons of the (OEP)In and the singlet at δ8.78 to Rh(OEP) *meso*-protons. The methylene and methyl protons are summarized in Table 2.

As evident from the chemical shifts in **I** and **IV**, the differences in chemical shifts of protons belonging to the In or the Rh porphyrin are more sig-

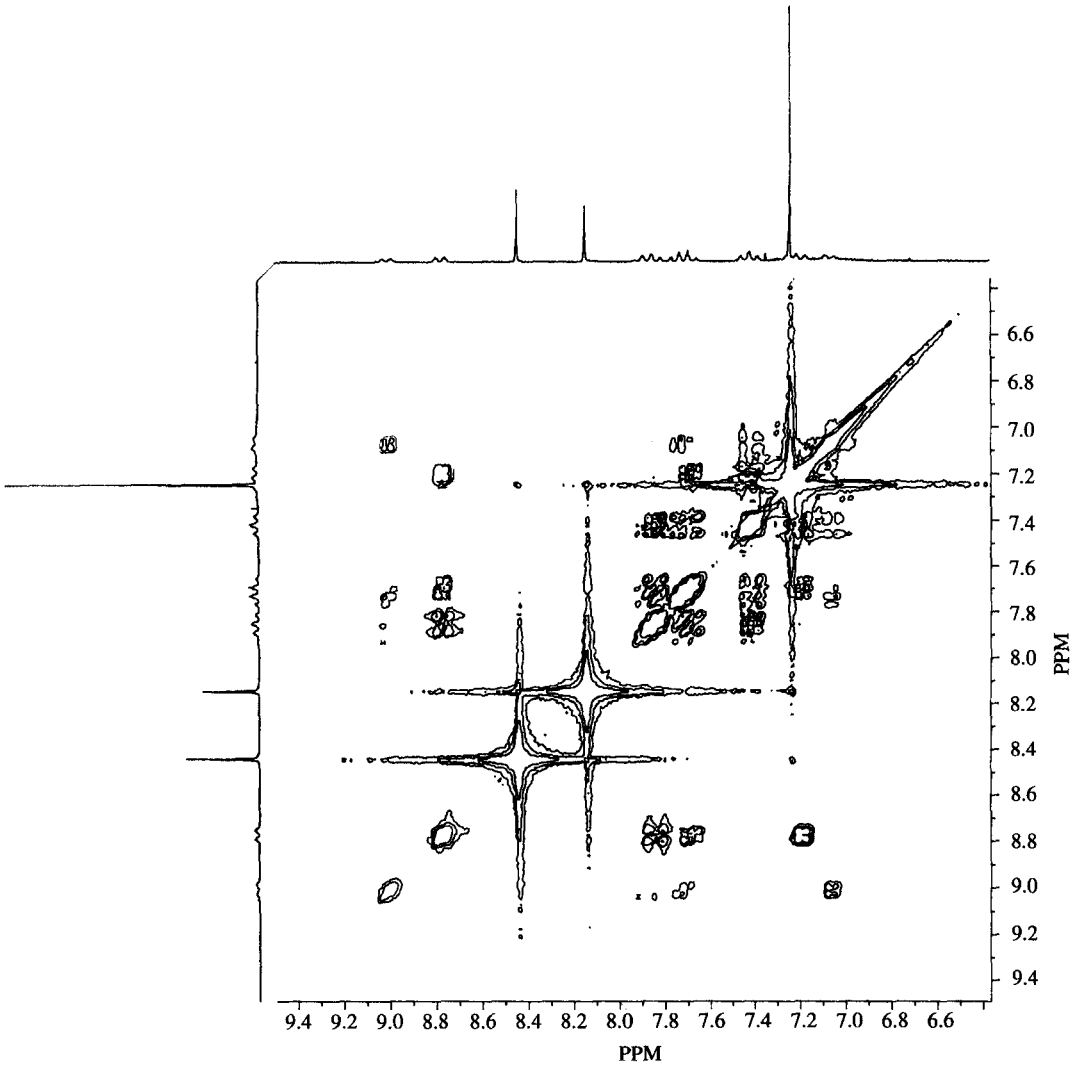

Fig. 3. COSY LR spectra of complex **IV** in $CDCl_3$.

Table 3. ^1H NMR literature data for complexes $(Por)_2M$, $M_2(Por)$, $(PorM)_2$, and (Por)(Por′)M

Compound	Solvent	*o′*-	*p*-	*m′*-	*m*-	*o*-	pyr	*p*-CH_3	*meso*	CH_2-	CH_3-
$(MoOEP)_2$	C_6D_6								9.2	4.32/3.92	1.78
$(MoTTP)_2$	C_6D_6	9.63		7.80	7.09	7.09	8.85	2.57	9.2	4.32/3.92	1.78
$(MoTPP)_2$	$CDCl_3$	9.28	7.77	7.92	7.38	6.90	8.51				
$(RhOEP)_2$	C_6D_6								9.23	4.40/3.90	1.68
$(RhTPP)_2$	C_6D_6	9.7	7.6	7.8	7.3	7.2	8.7				
$(RhTTP)_2$	C_6D_6	9.69		7.8	7.25	7.13	8.68	2.45			
$Ce(OEP)_2$	Toluene								9.11	4.2/3.86	1.68
									9.05	4.24/3.88	1.36
Ce(OEP)(TPP)	C_6D_6	9.68	7.72	8.25	7.25	6.4	8.18				
$Ce(TPP)_2$	$CDCl_3$	9.61	7.66	8.11	7.10	6.38	8.32				
$Ce(TTP)_2$	$CDCl_3$	9.39		7.89	6.96	6.24	8.12	2.57			
DPB	$CDCl_3$								8.95	4.15/3.8	1.75
Mo_2DPB	C_6D_6								9.25	4.4/3.9	1.6

nificant for the *o*-, *o'*-, and pyrrole protons for TPP and rise to 0.5 ppm for *meso*-protons in OEP. These differences are explained by the change of distance of the porphyrin protons from the centre of the magnetic anisotropy of the metal–metal bond due to displacement of the In atom from the porphyrin plane by *ca* 0.8 Å and the polarization of the In—Rh bond.[6] The orientation of the phenyl rings may also be different in the two porphyrins. The "bending" of the phenyls ought to be more important in (OEP)In because of the displacement of the metal out of the ring, also causing differences between (TPP)Rh protons chemical shifts.

Comparison of the chemical shift of the Rh(TPP) phenyl protons in **III** and **IV** reveals a weak shielding of 0.23 ppm for the *o'*- and 0.30 for the *m'*-(*endo*) phenyl protons belonging to the **IV** complex. This shielding is due to the presence of the phenyl rings of the (TPP)In macrocycle in **IV** and is clearly observed only for the *o'*- and *m'*-protons as they are located on the shielding region of the phenyl ring close to the ring centre. From the magnitude of this shielding the rotation of the (TPP)Rh fragment relative to the (TPP)In can be estimated using the description of the phenyl ring current effects proposed by Johnson and Bovey.[14] Using crystallographic data[6] for the (OEP)Rh–In(OEP) dimer for the interplanar distance, the metal–metal bond and the rotation angle (21.8°), molecular models were constructed[15] where the porphyrin rings were slightly domed.[6,16] The calculated shielding from the Johnson and Bovey model was 0.18 ppm for *o'*- and 0.40 ppm for *m'*-protons, in good agreement with the observed chemical shifts, suggesting that even in the case of the (TPP)In–Rh(TPP) complex, where the steric effects are important because of the neighbouring phenyl rings, the metal–metal bonds adopt the staggered conformation. This has also been observed for similar porphyrine complexes containing quadruple bonds.[17]

It is also interesting to compare the chemical shifts of these complexes with $[Rh(TPP)]_2$, $[Rh(OEP)]_2$,[6,12,13,16] and complexes exhibiting the same relative orientation of the two porphyrin rings but not containing any metal–metal bond, as in the Ce(IV) double deckers[15,19] (Table 3). The small differences observed between the chemical shifts of the protons of the different complexes suggests that the presence of the second porphyrin ring is the main centre of the magnetic anisotropy resulting in the deshielding (relative to monomers) for the *o'*-, (*endo*) protons and the shielding of the *o*-, (*exo*) protons. The presence of the metal–metal bond seems to have a weak influence, as suggested also from the chemical shifts of the *meso*-protons of DPB[20] and $Mo_2(DPB)$[21] (Table 3). Considering that these weak differences in chemical shift may also be the consequence of deformations of the porphyrin macrocycle, we believe that the magnitude of these differences is not significant in drawing conclusions about the metal–metal bond anisotropy.

Acknowledgments—This research was supported by the Greek General Secretary of Research and Technology through Grant No. 91EΔ442 and the Special Research Account of the University of Crete through the Research Commission (No. 149). Finally, we are grateful to Dr S. Georgiou for helpful discussions during this work.

REFERENCES

1. F. A. Cotton and R. A. Walton, *Multiple Bonds between Metal Atoms*. Clarendon Press, Oxford (1993).
2. H. Ogoshi, J. Setsune, T. Omura and Z. Yoshida, *J. Am. Chem. Soc.* 1975 **97**, 6461 and references therein.
3. (a) E Antonini and M. Brunori, *Hemoglobin and Myoglobin in their Reactions with Ligands*. North Holland Publishers, Amsterdam (1971); (b) W. S. Caughey, C. H. Barlow, D. H. O'Keefe and M. C. O'Toole, *Ann. N. Y. Acad. Sci.* 1973, **206**, 296; (c) W. S. Caughey, in *Inorganic Biochemistry* (Edited by G. 1. Eichorn) Vol. 2. Elsevier, Amsterdam (1973).
4. J. A. Ibers, L. J. Pace, J. Martinsen and B. M. Hoffman, *Struct. Bonding* 1982, **50**, 1.
5. (a) P. J. Brothers and J. P. Collman, *Acc. Chem. Res.* 1986, **19**, 209; (b) R. Guilard, C. Lecomte and K. M. Kadish, *Struct. Bonding* 1987, **64**, 205; (c) R. Guilard and K. M. Kadish, *Comments Inorg. Chem.* 1988, **6**, 287.
6. N. L. Jones, P. J. Carroll and B. B. Wayland, *Organometallics*, 1986, **5**, 33.
7. S. S. Eaton and G. R. Eaton, *J. Am. Chem. Soc.* 1975, **97**, 3660.
8. E. B. Fleischer and N. Sadasivan, *J. Chem. Soc., Chem. Commun.* 1967, 159.
9. M. Gouterman, in *The Porphyrins* (Edited by D. Dolphin), Vol. III. (1978).
10. (a) P. Cocolios, PhD Thesis, 1984 and references therein: (b) A. G. Coutsolelos and R. Guilard, *J. Organomet. Chem.* 1983, **253**, 273.
11. A. G. Coutsolelos, D. Lux and D. Daphnomili, *Polyhedron*, 1994, **13**, 2367.
12. J. P. Collman, C. E. Barnes, P. N. Swepston and J. A. Ibers, *J. Am. Chem. Soc.* 1984, **106**, 3500.
13. (a) A. Tabard, R. Guilard and K. M. Kadish, *Inorg. Chem.* 1986, **25**, 4277; (b) J. P. Collman, J. M. Garner and L. K. Woo, *J. Am. Chem. Soc.* 1989, **111**, 8141.
14. C. E. Johnson and F. A. Bovey, *J. Chem. Phys.* 1958, **29**, 1012.
15. Models were constructed using the *HyperChem* program, version 3 (publisher: Hyper Cube) (1993).

16. C-H. Yang, S. J. Djugan and V. L. Goedken, *J. Chem. Soc., Chem Comm.* 1986, 1313.
17. J. P. Collman, J. M. Garner, R. T. Hembre and Y. Ha, *J. Am. Chem. Soc.* 1992, **114**, 1292.
18. J. W. Buchler, A. De Cian, J. Fischer, P. Hammerschmitt, J. Löffler, B. Scharbert and R. Weiss, *Chem. Ber.* 1989, **122**, 2219.
19. E. Davoras, G. Spyroulias, E. Mikros and A. G. Coutsolelos, *Inorg. Chem.* 1994, **33**, 3430.
20. C. K. Chang and I. Abdalmuhdi, *Angew. Chem., Int. Ed. Engl.* 1984, **23**, 164.
21. J. P. Collman, K. Kim and J. M. Garner, *J. Chem. Soc., Chem. Comm.* 1986, 1711.